CORROSION SCIENCE AND TECHNOLOGY, Vol.24, No.4(2025), pp.230~247 pISSN 1598-6462 / eISSN 2288-6524
[Research Paper] DOI: https://doi.org/10.14773/cst.2025.24.4.230

Prediction of Electrochemical Characteristics of Metallic Bipolar Plates for PEMFCs Using Machine Learning and Deep Learning Model

Dong-Ho Shin[1] and Seong-Jong Kim[2,†]

[1]*Mokpo National Maritime University, 91, Haeyangdaehak-ro, Mokpo-si, Jeollanam-do, 58628, Republic of Korea*
[2]*Division of Marine System Engineering, Mokpo National Maritime University, 91, Haeyangdaehak-ro, Mokpo-si, Jeollanam-do, 58628, Republic of Korea*

(Received August 12, 2025; Revised August 18, 2025; Accepted August 20, 2025)

In this research, machine learning and deep learning models were employed to develop a predictive model for the electrochemical characteristics of 316L stainless steel used in metallic bipolar plates of PEM fuel cells (PEMFCs). The results indicated that hydrogen ion concentration (pH) exhibited the strongest correlation with electrochemical characteristics, as determined through SHAP analysis, Spearman correlation analysis, and the random forest model. Furthermore, the interaction between hydrogen ion concentration and hydrofluoric acid significantly decreased corrosion resistance, while hydrogen peroxide enhanced corrosion resistance by forming an oxide film on the surface. When comparing the performance of the MLP, DNN_Adam, and ResNet_Nadam prediction models, the DNN and ResNet models outperformed the MLP model. This superior performance is attributed to the use of appropriate optimizers (Adam and Nadam) and Bayesian optimization techniques to identify the optimal hyperparameters for each model. Notably, the ResNet_Nadam model emerged as the best predictor of electrochemical characteristics, achieving the highest R^2 value and showing a difference of less than 10% between training and validation data loss in the learning curve. These findings suggest that a thorough understanding of the independent variable data and the application of optimal parameters can enhance the predictive performance of deep learning models.

Keywords: *Machine learning, Deep learning, Prediction of electrochemical characteristics, Metallic bipolar plate, PEMFCs*

1. Introduction

Hydrogen is a clean and abundant energy source that can contribute significantly to reducing carbon emissions [1-3]. Among the various hydrogen energy applications, polymer electrolyte membrane fuel cells (PEMFCs) are attracting attention as a technology that is well suited for mobility applications such as automotive, aviation and vessel due to their fast startup, high efficiency and low operating temperature [4].

PEMFCs are assembled from a variety of components, among which the bipolar plates play an important role [5,6]. Metallic bipolar plates have high mechanical strength and can be manufactured in relatively small thicknesses, and simple processing methods such as stamping can be applied to mass-produce them and reduce costs [7]. However, during fuel cell operation, corrosive ions such as sulfate and fluoride ions are released from the electrolyte. This causes oxide film formation and corrosion damage on the surface of the metallic bipolar plates, which reduces the efficiency of the fuel cell [8-11]. Therefore, it is important to predict the electrochemical characteristics of the metallic bipolar plates according to the operating environment to evaluate its service life.

Recently, machine learning and deep learning techniques using artificial neural networks have shown excellent performance in predicting the electrochemical characteristics of metals and evaluating their durability, which has attracted the attention of many researchers [12-17].

M. Aghaaminiha et al. compared RF, ANN, Support Vector Machines (SVM) and K nearest neighbors (KNN) among machine learning models to predict the corrosion rate of carbon steel over time and found the best model, with mean squared errors ranging from 0.005 to 0.093 [18]. Y. Diao et al. improved the prediction performance of RF model electrochemical characteristics by selecting

[†]Corresponding author: ksj@mmu.ac.kr
Dong-Ho Shin: Researcher, Seong-Jong Kim: Professor

and generating input features of independent variables through GBDT model and Kendall correlation analysis [19]. In particular, it was presented that the application scope of the model can be expanded through feature extraction of independent variables. Y. Guang et al. proposed a new deep learning model that combines DNN model and attention mechanism, and developed an electrochemical characteristics prediction model with excellent performance by minimizing the loss function using RMSprop optimizer [20].

Using these machine learning and deep learning models to predict the electrochemical characteristics of metallic bipolar plates is critical for evaluating the lifetime of polymer electrolyte membrane fuel cells, which is important from a cost and safety perspective. Notably, the influence of corrosive ions released from the electrolyte during fuel cell operation and the prediction of their electrochemical characteristics over time will play a major role in understanding the degradation mechanism of the metal separator.

In this research, various electrochemical characteristics data of 316L stainless steel were extracted from solutions simulating fuel cell operating environment using hydrogen ion concentration, hydrofluoric acid concentration and hydrogen peroxide concentration as independent variables. The machine learning model was then used to analyze the correlation and interaction between the independent variables and electrochemical characteristics. In addition, a deep learning model was used to identify a prediction model for time-dependent electrochemical characteristics.

2. Experimental method

2.1 Preparation of specimen

The specimens used in this research were 316L stainless steel, whose chemical composition is shown in Table 1. The specimens were machined to a size of 20 mm × 20 mm, ultrasonically cleaned in acetone and distilled water for 3 minutes each, and then dried in a vacuum dryer for 24 hours. Only a 1 cm^2 area was exposed using a dedicated holder.

2.2 Electrochemical experiments and description of data

To obtain data on the electrochemical characteristics of the fuel cell under various operating conditions, a three-electrode cell was constructed to perform potentiodynamic polarization experiments. The counter electrode and reference electrode were a platinum mesh with a size of 20 mm × 20 mm and a silver/silver chloride electrode (sat. 3.3 M KCl solution), respectively. The potentiodynamic polarization experiments were performed at a scan rate of 1 mV/s from -0.25 V to 1.6 V (vs. OCP) after 30 min stabilization. Various electrochemical characteristics were then extracted using the Tafel extrapolation method.

To investigate the influence of various operating environments on electrochemical characteristics changes, pH (2, 2.5, 3, 3.5, 4), hydrofluoric acid (0.1, 0.5, 1, 1.5, 2 ppm) and hydrogen peroxide (1000, 1500, 2000, 2500, 3000 ppm) were selected as independent variables. The pH was adjusted using 95 wt% sulfuric acid. In addition, the corrosion potential, corrosion current density, anodic Tafel slope, cathodic Tafel slope, polarization resistance and surface roughness according to the independent variables were taken as dependent variables. A total of 125 sets of data were obtained.

To predict the change in time-dependent electrochemical characteristics, solutions and cycles of potentiodynamic polarization experiments were used as independent variables. The solution was varied from pH 2 to 4 at 0.1 intervals, and a total of 50 cycles (50 h) of potentiodynamic polarization experiments (1 h per cycle) were performed for each pH variable. The corrosion potential, corrosion current density, anodic Tafel slope, cathodic Tafel slope, polarization resistance and current density at 0.6 V were then calculated and used as dependent variables. The data obtained are time series data, with a total of 1050 sets.

2.3 Data preprocessing and model training

The features in the acquired dataset have different scales (ranges), which affects model learning [21]. In particular,

Table 1. Chemical composition of 316L stainless steel (wt%)

Ni	Cr	Mo	C	Si	Mn	P	S	Cu	N	Fe
10.17	16.9	2.01	0.022	0.61	1.03	0.033	0.029	0.281	0.011	Bal.

when training a model using an ANN, the weight update is more stable when the data is between 0 and 1. Therefore, to reduce the scale difference, we normalized the data between 0 and 1 using MinMaxScaler. Then, we split the training and validation data in an 80:20 ratio for model training. In addition, pH as an independent variable is defined using the logarithm of the hydrogen ion concentration, so it was converted to an exponential range and utilized.

Correlation analysis was performed to investigate the influence on electrochemical characteristics. Among various correlation methods, Spearman correlation analysis, which can measure non-linear relationships based on the ranking of variables, was performed, and the results were extracted as heat maps. Then, machine learning techniques (RF, XGBoost, GBDT, KNN, SVM, MLP) were used to model the relationship between independent and dependent variables. Mean squared error (MSE) and coefficient of determination (R^2) were used to evaluate the performance on the validation data. Shapley additive explanation (SHAP) analysis was used to quantitatively calculate the contribution of the independent variables to the dependent variable [22]. In addition, an MLP model was used to predict the electrochemical characteristics as a function of hydrogen ion concentration. The MLP model consisted of two hidden layers, and the number of nodes in the first and second hidden layers was set to 100 and 50, respectively. ReLU was used as the activation function of the hidden layer, and the loss calculation and weights of the predicted and actual values were updated by backpropagation of the error.

Deep learning models were used to predict time-dependent electrochemical characteristics. The deep learning models used were Deep Neural Network (DNN) and Residual Neural Network (ResNet). The activation functions used in the DNN and ResNet models are defined in Relu and use linear activation. Deep learning models depict different performance depending on different parameters (number of hidden layers, number of nodes in the hidden layer, dropout rate, learning rate) [23]. Therefore, it is important to find the optimal hyperparameters to generate the best model. To solve this problem, Bayesian optimization, which are widely known for efficiently finding optimal values for high-dimensional functions, were used. To find the optimal hyperparameters, the number of hidden layers, number of nodes in the hidden layer, dropout rate and learning rate were explored in the following ranges: 2 to 5, 32 to 128, 0.1 to 0.5 and 0.0001 to 0.01, respectively. The optimizers used are Adam, RMSprop and Nadam. To evaluate and validate the generalization performance of the best model, K-Fold cross-validation was performed, and the performance was evaluated by calculating R^2 and standard deviation. The learning curve was then used to analyze the overfitting of the model.

3. Results and discussion

Fig. 1 presents a heatmap [24] of the Spearman correlation between the independent variable (red) and the dependent variable (blue). Numbers inside the heatmap close to 1 indicate a positive correlation, while numbers close to -1 indicate a negative correlation. Hydrogen ion concentration was strongly correlated with all electrochemical characteristics. In particular, it showed a strong positive correlation with corrosion current density and surface roughness of 0.98 and 0.91, respectively. However, corrosion potential and polarization resistance showed a strong negative correlation of -0.87 and –0.91, respectively. This is due to the difference in the meaning of the electrochemical characteristics. Corrosion current density increases with increasing hydrogen ion concentration (acidic environment) due to more active electrochemical reactions [25,26]. However, the corrosion potential is known to represent a more active potential [27]. Notably, the polarization resistance is inversely related to the corrosion current density, so the opposite trend is expected. This trend was similarly observed for hydrofluoric acid. However, the correlation was weaker due to the relatively low concentration. In the case of hydrogen peroxide, the corrosion potential presented a positive correlation. This is because hydrogen peroxide, a strong oxidizing agent, reacts with iron and chromium in 316L stainless steel to form Fe_2O_3 or Cr_2O_3 oxide film, which increases the corrosion potential [28,29]. As a result, the hydrogen ion concentration was found to have the greatest influence on the electrochemical characteristics and surface roughness of 316L stainless steel.

Fig. 2 is the SHAP summary plot to evaluate the effect of the independent variables on the dependent variable. The SHAP analysis was performed using the RF model,

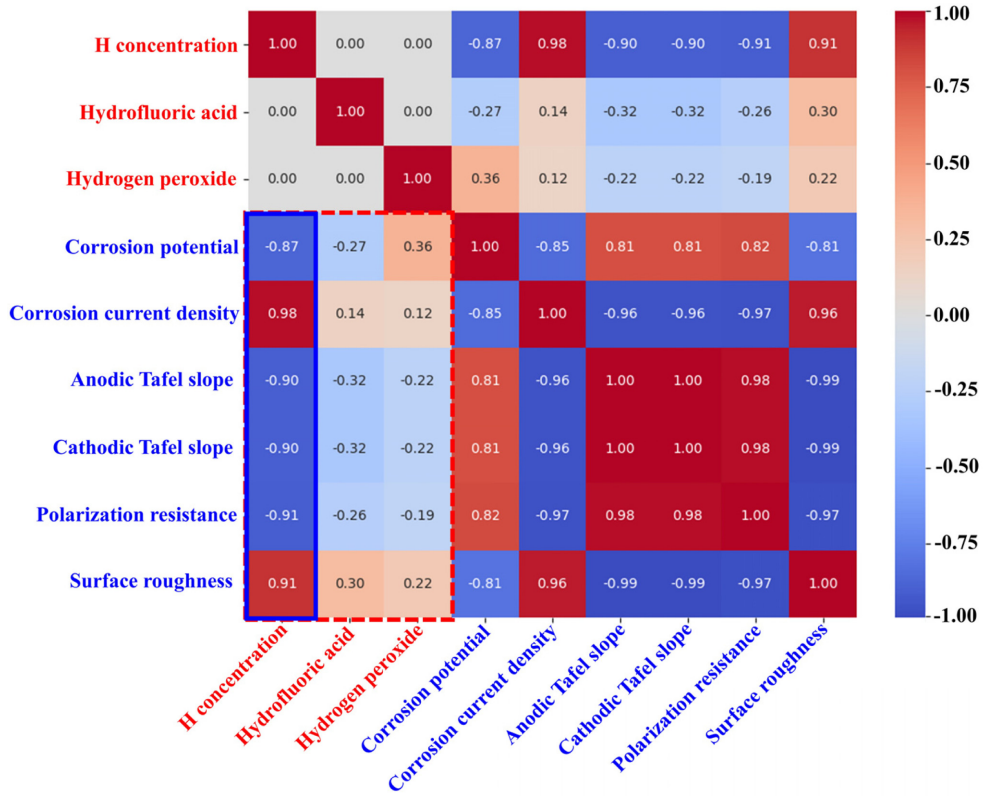

Fig. 1. Spearman correlation map of operating features for PEMFCs

which showed the best performance (highest R^2) among the RF, DT, XGBoost and GBDT models. In the SHAP summary plot, the X-axis shows the influence of the model on the output value (dependent variable) in terms of SHAP value, and the scale bar on the right (Feature value) demonstrates the size of the input value (independent variable, feature value). In the case of the scale bar, larger values are red color and smaller values are blue color. A positive SHAP value means that the input value increases the output value of the model, while a negative SHAP value means that it decreases the output value. A SHAP value of 0 (neutral) indicates that the input value has no effect on the output value. Also, the larger the absolute value of the SHAP value, the greater the influence of the corresponding independent variable.

For all outputs, the hydrogen ion concentration had the largest range of SHAP values, while hydrofluoric acid and hydrogen peroxide had relatively small values. This means that the hydrogen ion concentration has the greatest influence on electrochemical characteristics and surface roughness. In addition, the SHAP summary plot shape and trend of hydrofluoric acid and hydrogen peroxide concentrations were similar for the remaining outputs except for corrosion potential. This suggests the existence of a multicollinearity between hydrofluoric acid and hydrogen peroxide concentrations. Therefore, the variance inflation factor (VIF) was measured using only three independent variables, equation (1) is as follows.

$$\mathrm{VIF} = \frac{1}{1 - R^2} \tag{1}$$

In this equation, R^2 is the coefficient of determination calculated after regression analysis between independent variables.

The hydrogen ion concentration, hydrofluoric acid concentration, and hydrogen peroxide concentration used in this research were calculated as 1.618, 3.416, and 3.746, respectively. In general, variables with a VIF of 5 or higher are known to have multicollinearity problems. Therefore, the independent variables used in this research do not present multicollinearity. However, the similar shape and trend of hydrofluoric acid and hydrogen peroxide

concentrations is likely due to the similar properties of the data. In other words, the scale and distribution of the data are somewhat different when converted to ppm because the hydrogen ion concentration is a variable of pH. However, hydrofluoric acid and hydrogen peroxide concentrations in ppm have similar patterns. Therefore, it is considered that the VIF is relatively high compared to the hydrogen ion concentration, but since the value is small, there is no problem of multicollinearity.

In Fig. 2a, the SHAP value for corrosion potential increased with the decrease of hydrogen ion concentration. This indicates that the hydrogen ion concentration is inversely proportional to the corrosion potential. In particular, the change in corrosion potential (negative value) at high hydrogen ion concentration was more significant than the change for low hydrogen ion concentration. After the hydrogen ion concentration, the hydrogen peroxide concentration had the second largest effect on the corrosion potential, which also depicted a proportional relationship with the corrosion potential. This is believed to be due to the strong oxidizing properties of hydrogen peroxide, which formed an oxide film on the surface and increased the corrosion potential. The hydrofluoric acid concentration, which showed the smallest effect, presented a similar trend to the hydrogen ion concentration. In Fig. 2b, the input values all demonstrated a proportional relationship with the corrosion current density, and the high hydrogen ion concentration contributed significantly to the increase in SHAP value. On the other hand, hydrofluoric acid and hydrogen peroxide concentrations presented neutral SHAP values, and the change of SHAP value with the magnitude difference of input value was almost the same. Fig. 2c, d and e, the input values showed an inverse

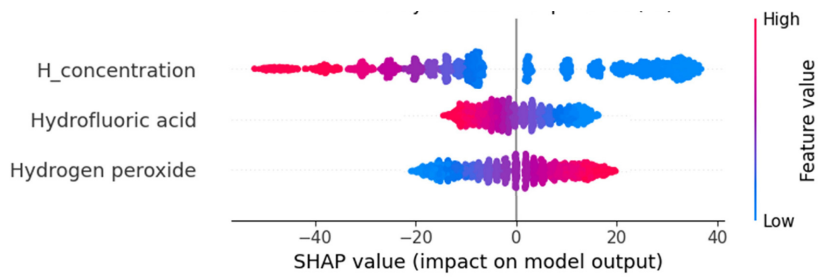

(a) Corrosion potential

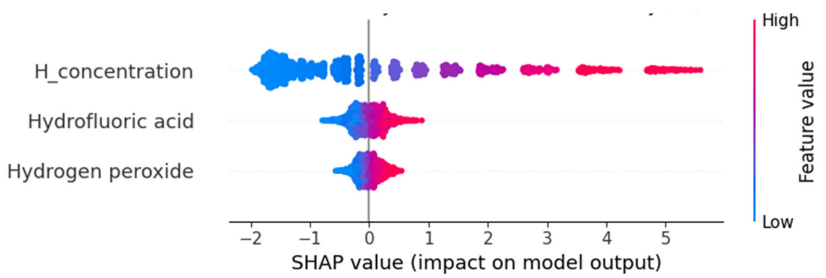

(b) Corrosion current density

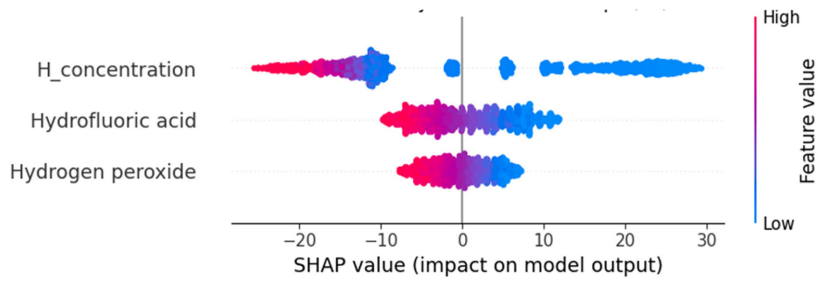

(c) Anodic Tafel slope

Fig. 2. Summary plot of datasets using SHAP values with Random Forest model

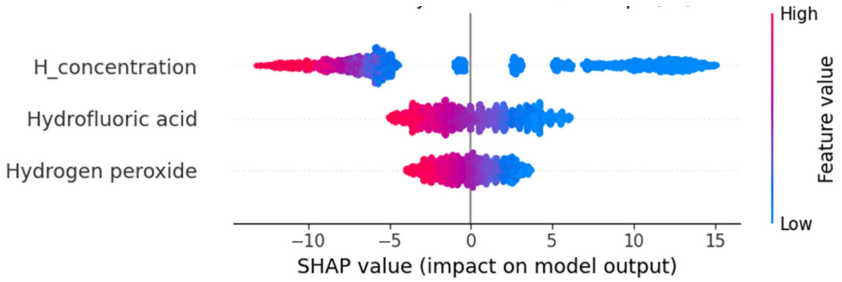

(d) Cathodic Tafel slope

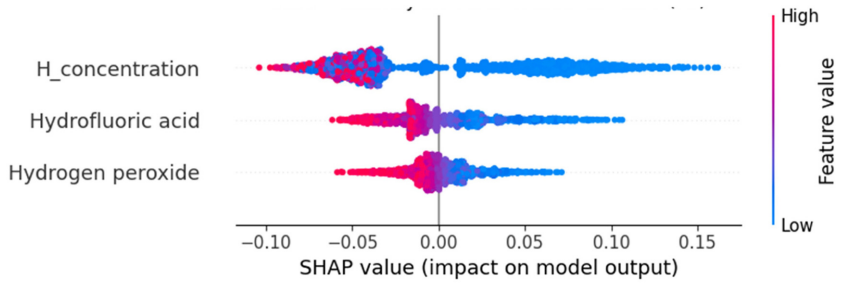

(e) Polarization resistance

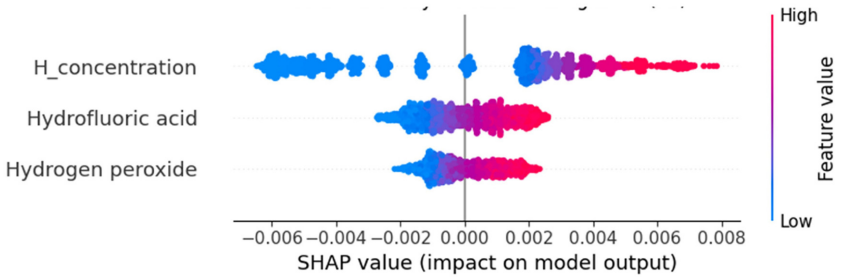

(f) Surface roughness

Fig. 2. (Continued) Summary plot of datasets using SHAP values with Random Forest model

relationship with the SHAP values for anodic Tafel slope, cathodic Tafel slope and polarization resistance, respectively. In general, the anodic and cathodic Tafel slope have a proportional relationship with corrosion resistance [30]. In other words, in electrolytes with a low hydrogen ion concentration, the electrochemical reaction is stable during polarization, and the change in current density is not large, so the Tafel slope is measured to be high. Therefore, it exhibits relatively superior corrosion resistance at low hydrogen ion concentration, resulting in high anodic and cathodic Tafel slope. In addition, polarization resistance also shows an inverse relationship with hydrogen ion concentration, and high polarization resistance indicates excellent corrosion resistance. As a result, the change in SHAP values (negative values) was the largest at low hydrogen ion concentration, which means that the decrease in hydrogen ion concentration has a significant effect on the increase in corrosion resistance. In the case of surface roughness in Fig. 2f, the trend was similar to the SHAP summary plot of corrosion current density, and the influence of hydrofluoric acid and hydrogen peroxide concentration was relatively large. This is because the surface damage of 316L stainless steel is clearly observed after the passivation period. In this research, the scanning range of the potentiodynamic polarization experiment was from the open-circuit potential to 1.6 V, and the surface damage in the transpassive region is dominant. In particular, it is known that pitting damage is more intense under mixed hydrofluoric acid and hydrogen peroxide conditions [31]. This is because the fluoride ions (F^-) contained in hydrofluoric acid penetrate into the oxide film formed by

hydrogen peroxide and accelerate localized corrosion. However, the corrosion current density is measured at the corrosion potential, which corresponds to a relatively low potential. Therefore, the electrochemical reaction by the hydrofluoric acid and hydrogen peroxide concentrations is thought to be relatively small. As a result, the corrosion current density and surface roughness showed similar trends, but the influence of the hydrofluoric acid and hydrogen peroxide concentrations showed differences. This is thought to be because the potential interacts with the hydrofluoric acid and hydrogen peroxide concentrations.

Fig. 3 presents the interaction of hydrogen ion concentration with hydrofluoric acid and the interaction of hydrogen ion concentration with hydrogen peroxide on corrosion current density using RF model. The interaction of concentration was analyzed and the results

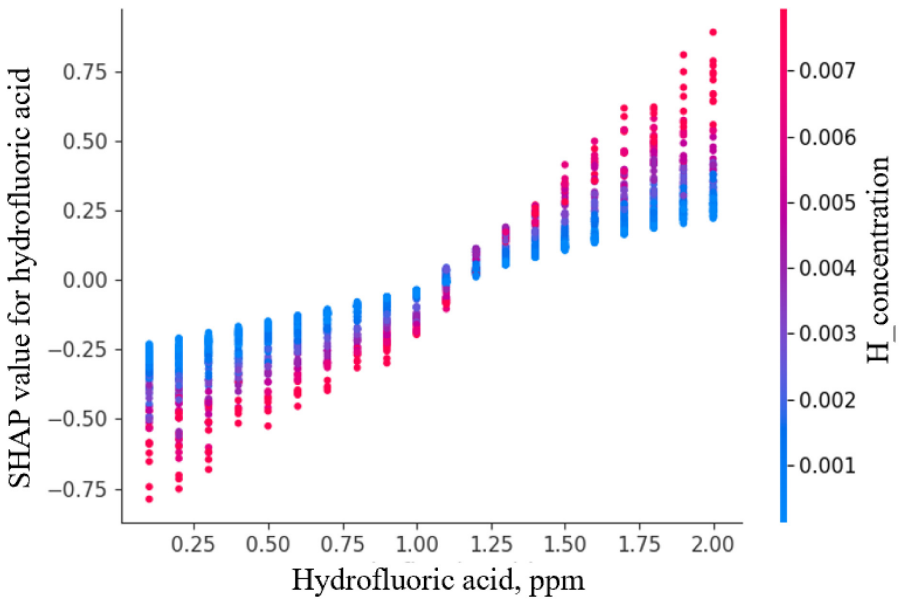

(a) Hydrofluoric acid

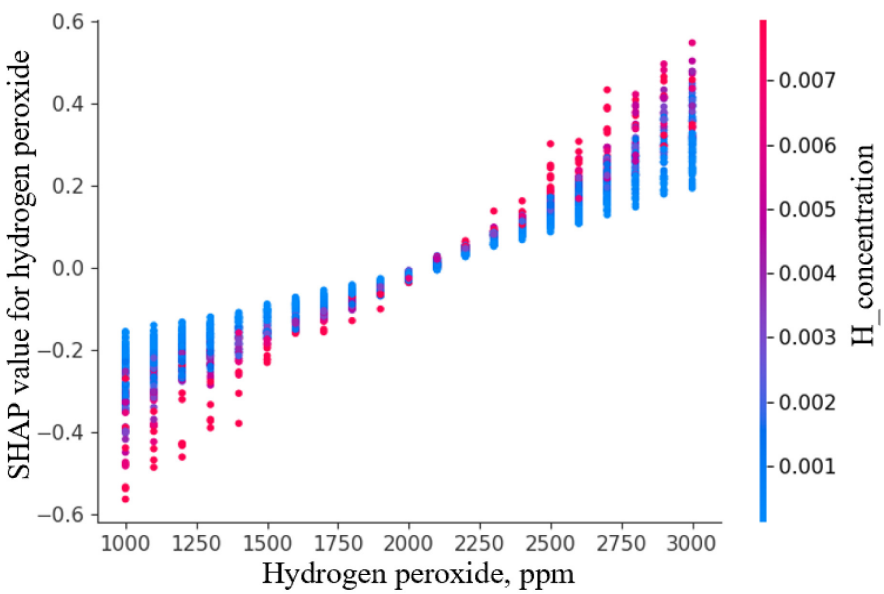

(b) Hydrogen peroxide

Fig. 3. SHAP dependence plot of hydrofluoric acid and hydrogen peroxide on corrosion current density using Random Forest model

are demonstrated as SHAP dependence plot. The X-axis represents the hydrofluoric acid and hydrogen peroxide concentrations, respectively. The Y-axis represents the SHAP value of the effect of hydrofluoric acid and hydrogen peroxide on the corrosion current density by interacting with the hydrogen ion concentration. The scale bar on the right indicates the magnitude of the hydrogen ion concentration. As shown in Fig. 3a, the SHAP value of corrosion current density with changing hydrofluoric acid concentration was significantly affected by the hydrogen ion concentration. That is, the blue points with low hydrogen ion concentration were mostly distributed near the SHAP value of 0 with the change of hydrofluoric acid concentration. However, the red points with high hydrogen ion concentration presented relatively high SHAP values. This indicates that the hydrogen ion concentration has a greater influence on the corrosion current density than the hydrofluoric acid concentration. This trend is similar to the dependence of hydrogen peroxide concentration on corrosion current density in Fig. 3b. However, compared to the hydrofluoric acid concentration plot, the SHAP value is relatively small. In other words, the interaction of hydrogen ion concentration and hydrofluoric acid concentration resulted in SHAP values for corrosion current density above about 0.75. However, the interaction of hydrogen ion concentration and hydrogen peroxide concentration indicated a SHAP value of about 0.6 or less, suggesting that the interaction of hydrogen ion concentration and hydrofluoric acid concentration has a greater effect on the corrosion current density. In general, fluoride ions contained in hydrofluoric acid are known to be halogen ions that destroy the oxide film on the metal surface and accelerate localized corrosion. These halogen ions react with the metal to accelerate pitting damage by self-propagating and autocatalytic reactions mechanisms. Hydrogen peroxide, on the other hand, is a strong oxidizing agent that forms an oxide film on the metal surface. Therefore, it is believed to alleviate the corrosion damage caused by hydrogen ion concentration. As a result, the hydrogen ion concentration, hydrofluoric acid and hydrogen peroxide used in this research were found to interact on electrochemical characteristics. In particular, hydrogen ion concentration and hydrofluoric acid further reduce the corrosion resistance, which is a factor that should be paid attention to during fuel cell operation.

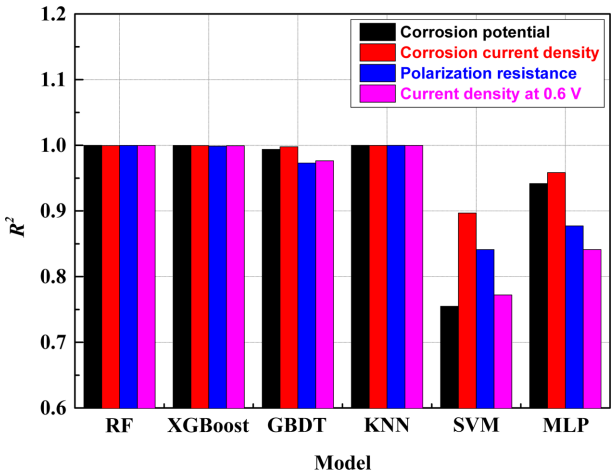

Fig. 4. Electrochemical characteristics prediction performance of Random Forest model (RF), eXtreme Gradient Boosting model (XGBoost), Gradient Boosting Decision Tree model (GBDT), K-Nearest Neighbor model (KNN), Support Vector Machine model (SVM) and Multi-layer Perceptron model (MLP)

Fig. 4 presents the results of predicting electrochemical characteristics using various learning models and calculating R^2 for performance evaluation. The RF, XGBoost, GBDT and KNN models show excellent prediction performance for all electrochemical characteristics. These models are powerful in learning relationships in non-linear data and can learn interactions between variables by utilizing the tree structure and local distribution of the data. However, SVM use a kernel trick to map the input data into a high-dimensional space and then use a linear hyperplane to separate the data [32]. This limits their ability to learn interactions between variables directly. Similarly, MLP is a multilayer neural network structure where neurons in the hidden layer are interconnected and can learn interactions through nonlinear transformations [33]. However, it requires optimal hyperparameter tuning by constructing an appropriate model structure. As mentioned earlier, the independent variables used in this research, hydrogen ion concentration, hydrofluoric acid and hydrogen peroxide, interact to influence the change of the electrochemical characteristics. Notably, hydrogen ion concentration and hydrofluoric acid further degraded the corrosion resistance, while hydrogen peroxide contributed to the formation of an oxide film on the surface, which resulted in relatively superior corrosion resistance. This may

explain the relatively poor performance of SVM and MLP models that have not been properly trained on interactions. As a result, machine learning models such as RF, XGBoost, GBDT and KNN are excellent predictive models. However, these models are known to have limitations in handling time series data and training the models. Some machine learning models, such as the ARIMA model, can effectively handle time series data and perform well in predicting the dependent variable [34]. Nevertheless, we believe that deep learning models with deeper structure can generate better predictive models for data that is complex or non-trending.

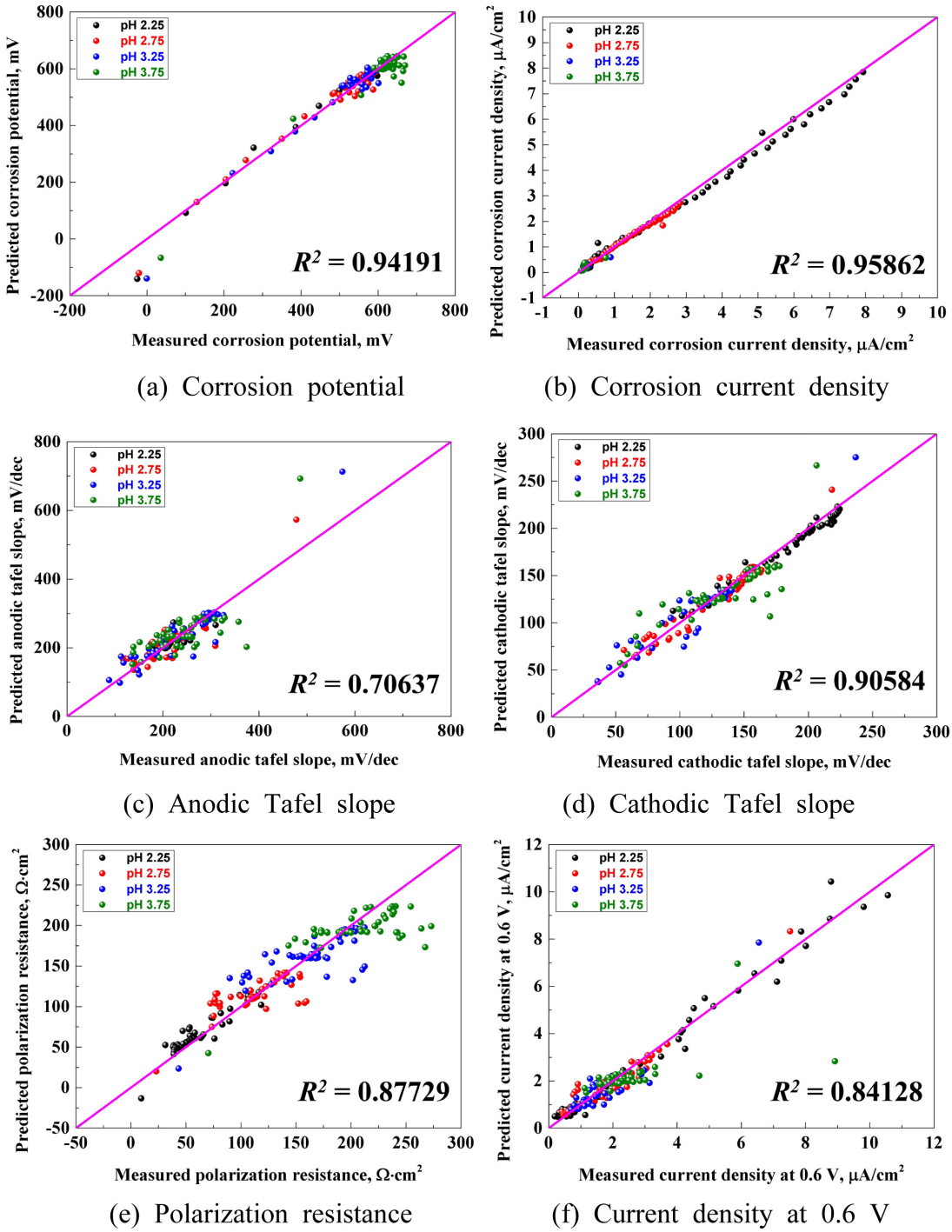

Fig. 5. Predictive accuracy of the electrochemical characteristics prediction model with MLP model

Fig. 5 depicts the results of electrochemical property predictions for hydrogen ion concentrations of 5.62×10^{-3} (pH 2.25), 1.78×10^{-3} (pH 2.75), 5.62×10^{-4} (pH 3.25) and 1.78×10^{-4} (pH 3.75) using the MLP model among the deep learning models. The dataset used to train the predictive model is electrochemical experimental data obtained by performing 50 cycles of potentiodynamic polarization experiments at 0.1 intervals from pH 2 to 4. MLP models are based on multi-layer artificial neural networks with multiple hidden layers [35]. Typically, the first layer learns low-level features with a large number of nodes. This is to ensure that the initial layer learns enough data. The number of nodes is then reduced in subsequent layers to reduce computational cost and training time. In particular, the number of nodes can be reduced as the number of hidden layers increases to prevent overfitting [36]. The results of training and validation for the predictive model show that the actual and predicted values for all electrochemical characteristics are linear, resulting in a high R^2. In particular, corrosion potential, corrosion current density and cathodic Tafel slope presented significantly higher R^2 than 0.9. However, the anodic Tafel slope, polarization resistance and current density at 0.6 V depicted relatively low R^2. The difference in R^2 between anodic and cathodic Tafel slopes is attributed to changes in the metal surface due to electrochemical reactions [37]. In general, in acidic solutions, metal surfaces change their electrochemical characteristics due to oxide film formation and corrosion damage. This is more pronounced and persistent during anodic polarization from the open circuit potential (oxidation reaction). On the other hand, the cathodic characteristics also change depending on the surface change, but the trend is not significant. This is because the reduction reaction is dominant at cathodic polarization, and the surface change is relatively small. Therefore, the cathodic polarization has a similar trend, which is considered to be the reason for the high accuracy of the predictive model. These results are similar for the predictive model of current density at 0.6 V. At relatively high potentials, the R^2 of the predictive model is low due to the breakdown of passive film and transpassivation characteristics of the passivation film, which prevent the actual measurements from showing a clear linearity. This is due to uncontrollable variables that occur during the experiment. In particular, depending on the presence and extent of defects on the specimen surface, the current density may vary due to strong oxidation reactions (corrosion reactions, large anodic polarization) [38].

Fig. 6 presents the results of training and validation of a predictive model of electrochemical characteristics with a deep learning model using time series data according to the pH variable. The models were selected as DNN and ResNet, and the parameters were set as the number of nodes (10 to 128), number of hidden layers (1 to 5), dropout rate (0.1 to 0.5) and learning rate (0.0001 to 0.01) using Bayesian optimization technique, respectively. The initial search and iteration numbers were set to 10 and 30, respectively, and the optimal hyperparameters were explored. The performance was then evaluated by R^2 as a function of the ratio of optimizer and training data. DNN is an extension of MLP, which is designed to learn simple patterns of data in the initial layer and higher-dimensional patterns in subsequent layers, so that it can learn the overall correlation of data [39]. However, if there are too many hidden layers (deepening), the vanishing gradient of the loss function occurs during backpropagation, resulting in slow learning speed and overfitting. To avoid these problems, the ResNet model was devised [40]. It is a deep learning model based on residual learning that does not degrade as the depth of the neural network (hidden layer) increases. An optimizer is an algorithm that appropriately updates the weights and biases in training the model [41]. Notably, it calculates the loss values of

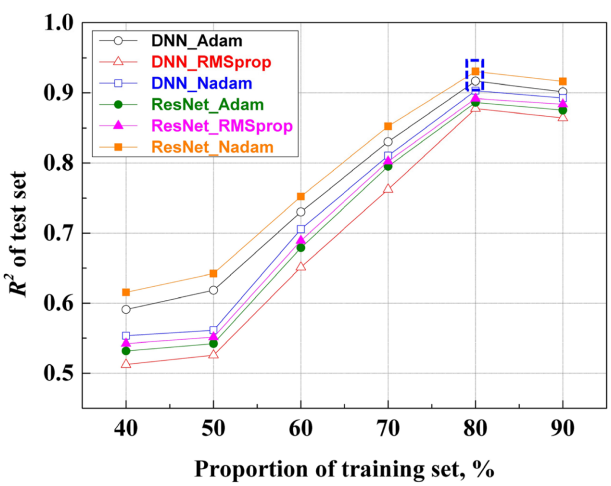

Fig. 6. Electrochemical characteristics prediction performance of Deep Neural Network (DNN) and Residual Neural Network (ResNet) with Adam, RMSprop, Nadam optimizer

the training and validation data and finds the optimal hyperparameters at each iteration to minimize the loss function and converges. The optimizers used in this research are Adam, RMSprop and Nadam. Adam tracks the first moment (mean) and second moment (variance) of the gradient vector of the training data to calculate the learning rate and loss function, and adjusts the parameters according to the results [42]. RMSprop adjusts the learning rate by calculating an exponential moving average of the squared loss function gradient [43]. Nadam is a method that combines Adam with the Nesterov momentum technique with lookahead capability to estimate the gradient of the loss function and pre-assign the necessary weights [44]. It estimates the loss function faster and more efficiently than traditional Adam, allowing for faster parameter convergence. Independent of the model and optimizer, R^2 increased as the proportion of training data increased. In particular, R^2 increased sharply for the proportion of training data above 60%. This indicates that the performance of the predictive model increases as the training data increases and the validation data decreases. This increase was evident up to 80% of the training data. In general, increasing the proportion of training data is effective for extracting correlations between independent and dependent variables. It also improves the generalization capability of the model [45]. However, at 90% of the training data, a decrease in the performance of the predictive model was observed. This is due to the overfitting of the predictive model with a high proportion of training data. The performance comparison by model and optimizer presented that the Adam optimizer performed the best in the DNN model. On the other hand, Nadam performed the best in the ResNet model. In particular, the ResNet_Nadam model showed the highest R^2 in all training data proportion conditions, suggesting that it is the best model for predicting time-dependent electrochemical characteristics. The differences in the best optimizers for different models are due to the characteristics and suitability of the models and optimizers. DNNs have the simplest structure among deep learning models, with all data trained on the same path. However, they suffer from gradient loss as the hidden layer grows. Adam mitigates the gradient descent problem by speeding up the initial training. For this reason, Adam seems to produce the best predictive models when applied to DNN models. ResNet, on the other hand, uses residual learning, which means that the learning path is complex and the magnitude and direction of the gradient can vary. This leads to instability in the slope of the loss function. However, when using the Nadam optimizer combined with the Nesterov technique, the look-ahead feature is applied to reduce the instability of the gradient and lead to a more stable convergence. As a result, the training data proportion of 80% in DNN_Adam and ResNet_Nadam was selected as the training condition for prediction of the electrochemical characteristics.

Fig. 7 and Table 2 present the results of prediction and validation of electrochemical characteristics using Adam optimizer for DNN model with training data proportion of 80 %. In order to learn a better prediction model, we changed the number of nodes and the number of hidden layers in the previous optimization technique to a range of 32 to 128 and 2 to 5, respectively, and increased the number of initial exploration and iterations to 50 and 100, respectively. This is to increase the efficiency of the optimal hyperparameter search, improve the reliability of the search results and the performance of the predictive model. DNN_Adam depicted a excellent performance predictive model for all electrochemical properties. In particular, a significant increase in R^2 of corrosion current density was observed compared to the MLP model. The data distribution was highly skewed for all pH conditions. This is likely due to the effect of time in cycling experiments. Initially, the potentiodynamic polarization experiment presented relatively low corrosion potential and high corrosion current density due to the instability of the oxide film formed in the atmosphere. However, as cycles (time) passed, a denser oxide film was formed on the surface, which tended to increase the corrosion

Table 2. DNN_Adam model performance of cycle dataset

	MAE	MSE	RMSE	R^2
Corrosion potential	20.126	946.25	30.761	0.949
Corrosion current density	0.127	0.028	0.171	0.981
Anodic Tafel slope	23.903	1241.394	35.233	0.715
Cathodic Tafel slope	9.803	203.745	14.273	0.922
Polarization resistance	17.144	593.300	24.357	0.890
Current density at 0.6 V	0.516	0.610	0.781	0.875

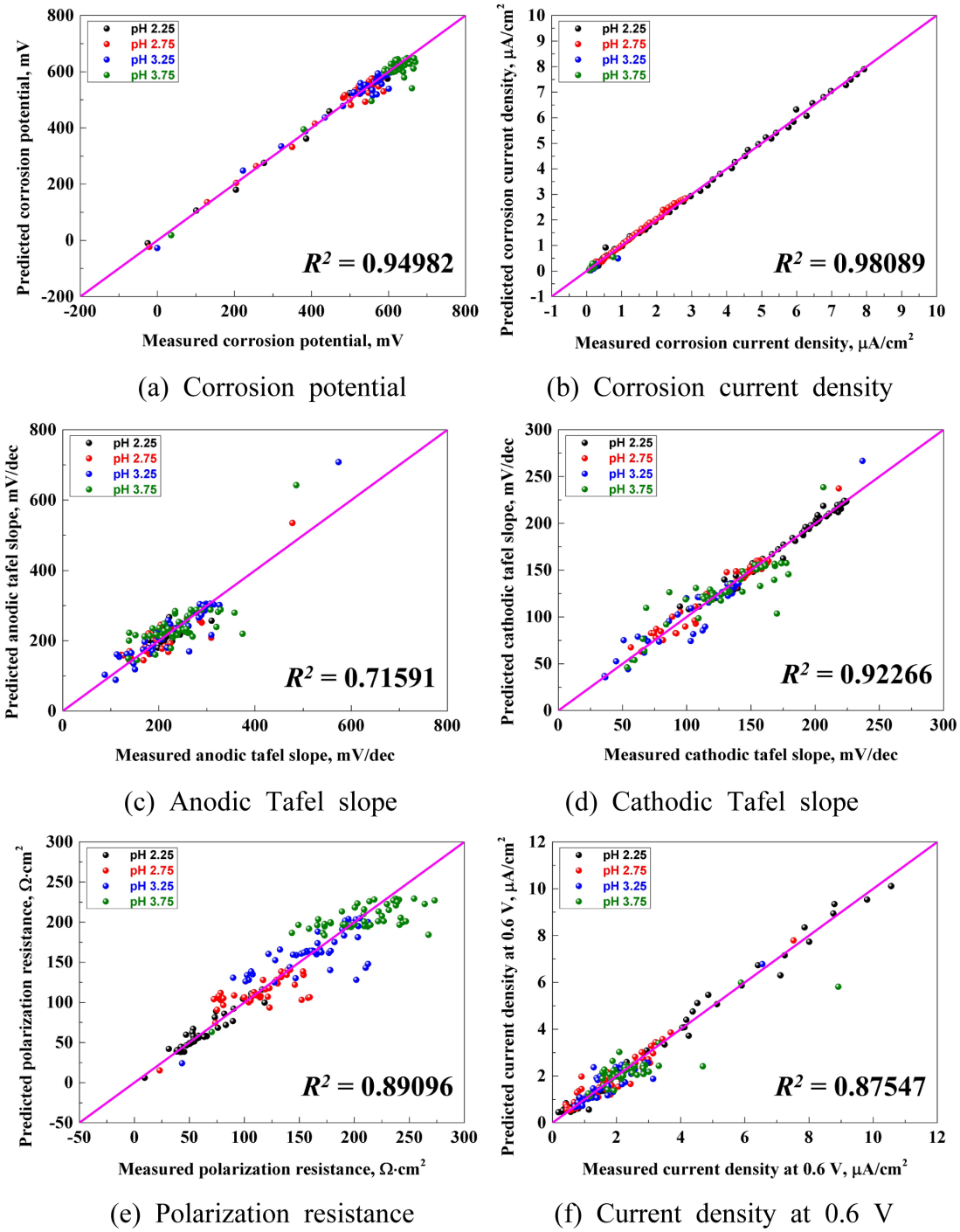

Fig. 7. Predictive accuracy of the electrochemical characteristics prediction model with DNN_Adam model

potential and decrease the corrosion current density [46]. Therefore, the distribution of experimental data is considered to be large. In particular, when the pH is low, the electrochemical reaction is more active and the change in electrochemical characteristics is large [47]. Also, for polarization resistance and current density at 0.6 V, the actual and predicted values showed a relatively strong linearity at low pH. However, the linearity decreased at higher pH. This is similar to the SHAP summary diagram results for polarization resistance in Fig. 2. That is, the range of output values of polarization resistance was larger at higher pH than at lower pH. This is likely due to

variables such as the initial state of the specimen at high pH conditions having a greater influence on the electrochemical characteristics.

Fig. 8 and Table 3 demonstrate the results of prediction and validation for electrochemical characteristics using the Nadam optimizer in the ResNet model. Compared to the previous two models (MLP and DNN), the performance of the predictive model for all electrochemical characteristics is improved. Notably, the corrosion current density presented an R^2 of 0.99624, indicating a excellent prediction accuracy. The linearity at high pH increased compared to MLP and DNN. This is because the combination of the

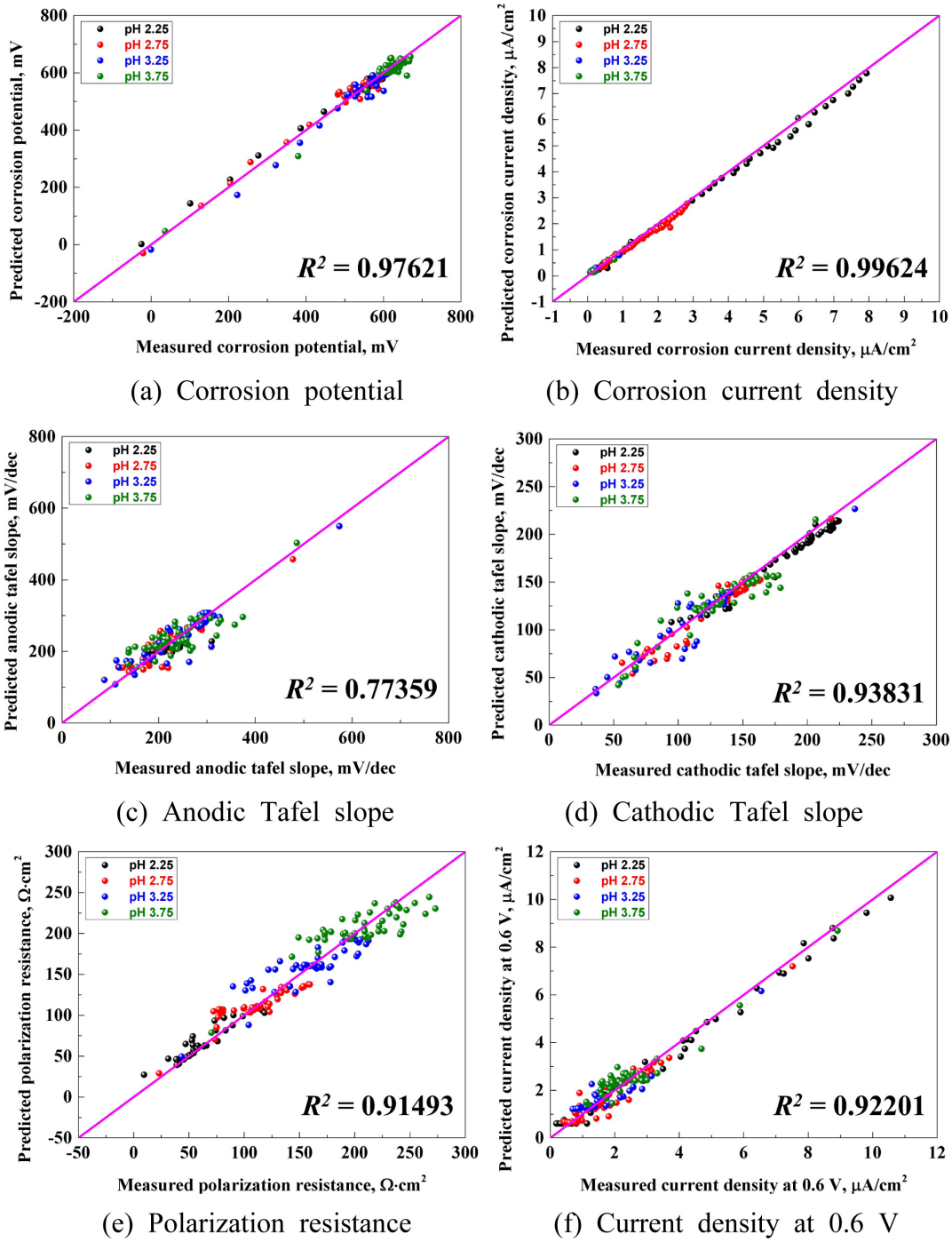

Fig. 8. Predictive accuracy of the electrochemical characteristics prediction model with ResNet_Nadam model

Table 3. ResNet_Nadam model performance of cycle dataset

	MAE	MSE	RMSE	R^2
Corrosion potential	18.022	612.677	24.752	0.976
Corrosion current density	0.096	0.020	0.143	0.996
Anodic Tafel slope	24.393	1189.832	34.493	0.773
Cathodic Tafel slope	9.630	161.290	12.700	0.938
Polarization resistance	16.363	512.203	22.631	0.914
Current density at 0.6 V	0.382	0.481	0.668	0.922

ResNet model and the Nadam optimizer more accurately predicts the direction of change in the slope and converges stably to the hyperparameters for training the predictive model.

Among the deep learning models used in this research, the ResNet_Nadam model showed the best performance. The ResNet model's structure effectively overcomes the gradient vanishing problem that can occur in deep neural networks through residual learning, and the Nadam

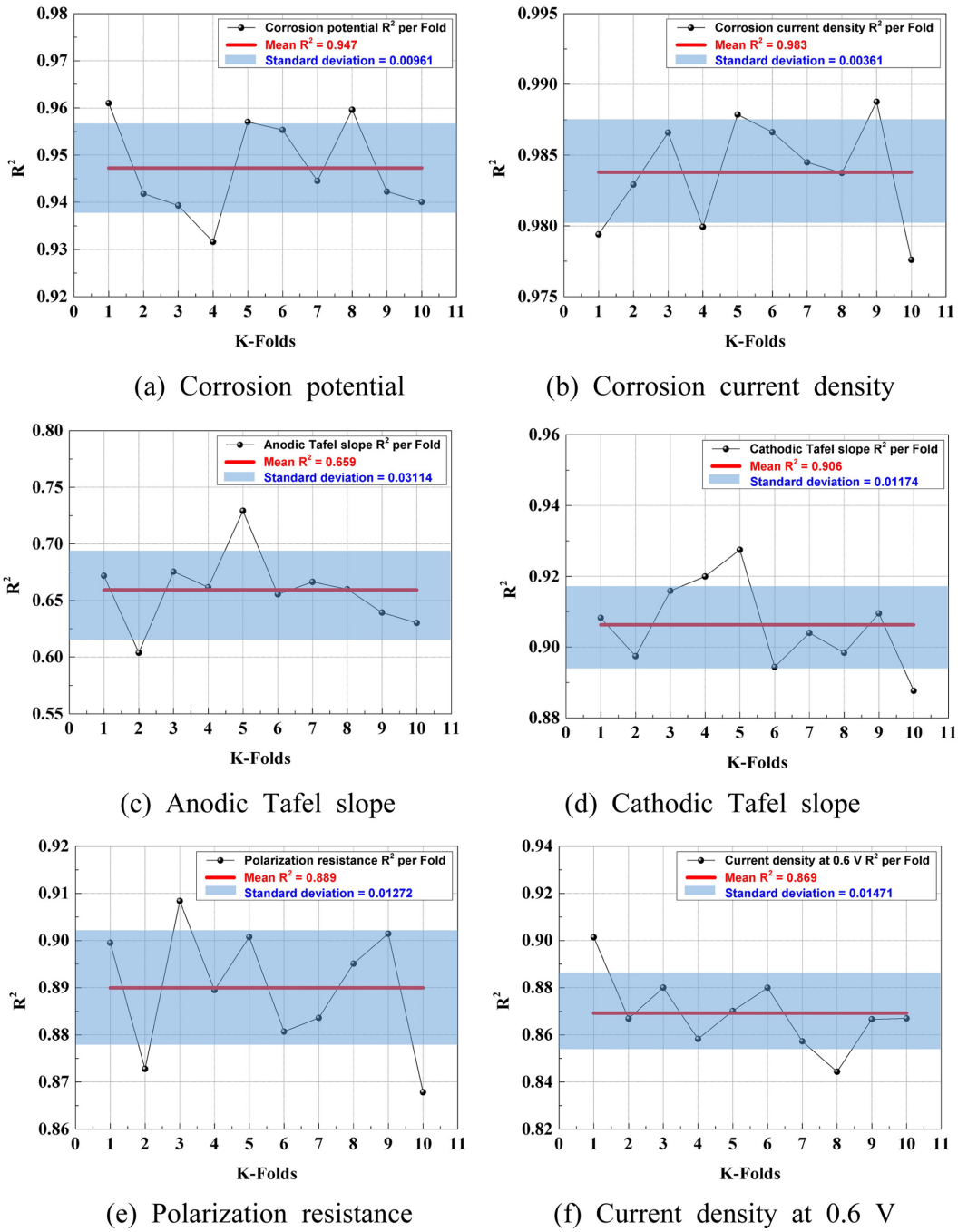

(a) Corrosion potential (b) Corrosion current density

(c) Anodic Tafel slope (d) Cathodic Tafel slope

(e) Polarization resistance (f) Current density at 0.6 V

Fig. 9. K-Fold cross-validation comparison of ResNet_Nadam model

optimizer simultaneously improves convergence stability and prediction accuracy during the learning process by combining the Nesterov momentum and Adam algorithms. These structural and mathematical characteristics have been shown to be highly compatible with nonlinear electrochemical data and highly effective in learning highly volatile time-series data. In particular, the model showed excellent performance in predicting various electrochemical characteristics according to pH. Furthermore, pH was found to have the greatest influence on corrosion acceleration of 316L stainless steel, which was consistent with the results of Spearman correlation analysis and SHAP analysis.

Fig. 9 presents the generalization performance of the ResNet_Nadam model using K-Fold cross-validation. K-Fold cross validation makes the best use of existing data by splitting the data to use as training and validation data when the dataset is insufficient. In particular, it can evaluate whether the model is overfitting or not by iteratively splitting the training and validation data. The black points show the predictive performance (R^2) of the ResNet_Nadam model as a function of fold, the red line shows the mean of R^2, and the blue box depicts the standard deviation of R^2. For all electrochemical characteristics, the standard deviation is less than 0.05, indicating excellent generalization performance of the predictive model. In particular, for corrosion potential and corrosion current density, the standard deviation was less than 0.01, indicating the best prediction performance.

Fig. 10 is a learning curve that quantitatively evaluates the loss of training and validation data during the training process of ResNet_Nadam's prediction model according to the number of iterations (epochs). The X-axis represents the number of iterations in the learning process, and the Y-axis represents the loss function value. The loss function for the training data started at a high value of 0.34 and decreased rapidly as the number of epochs increased. For the validation data, the loss function started at a low value and decreased as the epoch increased, but did not present a significant difference. The loss functions of the training and validation data had similar values from about 20 epochs, with less than 10% difference between 40 and 50 epochs. In general, if the difference between the loss function values of training and validation data in the learning curve is more than 20%, it is classified as

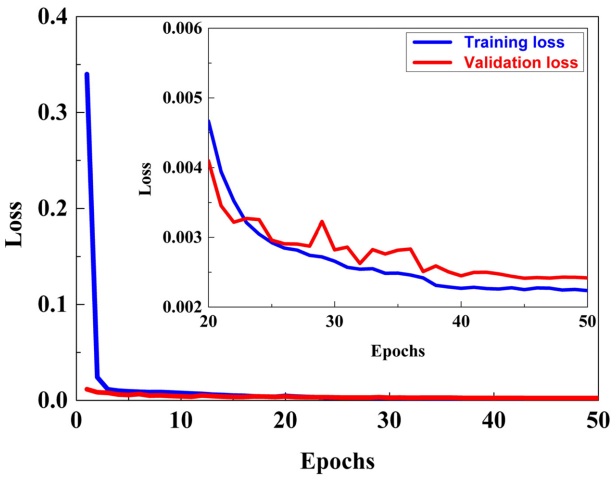

Fig. 10. Learning curve of ResNet_Nadam model

overfitting (training data loss < validation data loss) or underfitting (training data loss > validation data loss) [48]. The prediction model using ResNet_Nadam shows excellent performance due to the low difference in loss function values.

4. Conclusions

Machine learning and deep learning techniques were used to predict the electrochemical characteristics of 316L stainless steel for PEMFCs metallic bipolar plates, and the results are as follows.

Spearman correlation analysis and SHAP analysis presented that the hydrogen ion concentration (pH) had the strongest correlation with all electrochemical characteristics. In particular, pH had a significantly greater effect on corrosion current density compared to hydrofluoric acid and hydrogen peroxide concentrations. High hydrogen ion concentration significantly increased the SHAP value of corrosion current density. On the other hand, the SHAP value decreased at low hydrogen ion concentration, but the magnitude was relatively small. Hydrogen ion concentration and hydrofluoric acid concentration interacted to decrease corrosion resistance. However, hydrogen peroxide had the effect of increasing the corrosion resistance by forming an oxide film on the surface.

When comparing the performance of MLP, DNN_Adam and ResNet_Nadam, the DNN and ResNet models performed better than MLP. This is due to the Bayesian

optimization technique and the search for optimal hyperparameters by selecting appropriate optimizers. In particular, ResNet_Nadam was the best predictive model for electrochemical property prediction with the highest R^2. The difference between training and validation data loss in the learning curve was less than 10%.

As a result, it is important to explore the optimal optimizers and hyperparameters according to the model to improve the performance of deep learning models. In particular, understanding the various characteristics of data (linearity, non-linearity, interactivity of independent variables, etc.) and selecting and applying optimal parameters can significantly improve the prediction performance of deep learning models.

References

1. S. Evro, B. A. Oni, and O. S. Tomomewo, Carbon neutrality and hydrogen energy systems, *International Journal of Hydrogen Energy*, **78**, 1449 (2024). Doi: https://doi.org/10.1016/j.ijhydene.2024.06.407
2. W. S. Yang, J. H. Kim, J. Lee, and S. J. Kim, Comparison study of polymer and Ti sol-gel carbon coating on Ti for PEMFC bipolar plates, *Corrosion Science and Technology*, **22**, 447 (2023). Doi: https://doi.org/10.14773/cst.2023.22.6.447
3. L. Fan, Z. Tu, and S. H. Chan, Recent development of hydrogen and fuel cell technologies: A review, *Energy Reports*, **7**, 8421 (2021). Doi: https://doi.org/10.1016/j.egyr.2021.08.003
4. G. Varghese, V. Babu K. P., T. V. Joseph, and P. Chippar, A numerical investigation on thermal gradients and stresses in high temperature PEM fuel cell during start-up, *International Journal of Heat and Mass Transfer*, **175**, 121365 (2021). Doi: https://doi.org/10.1016/j.ijheatmasstransfer.2021.121365
5. D. H. Shin and S. J. Kim, Effects of temperature and chloride concentration on electrochemical characteristics and damage behavior of 316L stainless steel for PEMFC metallic bipolar plate, *Corrosion Science and Technology*, **21**, 300 (2024). Doi: https://doi.org/10.14773/cst.2022.21.4.300
6. K. H. Kim, J. W. Lim, M. Kim, and D. G. Lee, Development of carbon fabric/graphite hybrid bipolar plate for PEMFC, *Composite Structures*, **98**, 103 (2013). Doi: https://doi.org/10.1016/j.compstruct.2012.10.043
7. Q. Hu, D. Zhang, H. Fu, and K. Huang, Investigation of stamping process of metallic bipolar plates in PEM fuel cell - Numerical simulation and experiments, *International Journal of Hydrogen Energy*, **39**, 13770 (2014). Doi: https://doi.org/10.1016/j.ijhydene.2014.01.201
8. H. Tawfik, Y. Hung, and D. Mahajan, Metal bipolar plates for PEM fuel cell - A review, *Journal of Power Sources*, **163**, 755 (2007). Doi: https://doi.org/10.1016/j.jpowsour.2006.09.088
9. Y. H. Kim, J. S. Park, and S. J. Kim, Comparative study of corrosion resistance of organic coating and dry coating on 304 stainless steels used for bipolar plates in polymer electrolyte membrane fuel cells, *Corrosion Science and Technology*, **22**, 242 (2023). Doi: https://doi.org/10.14773/cst.2023.22.4.242
10. H. S. Heo and S. J. Kim, Electrochemical characteristics of MMO (Ti/Ru)-coated titanium in a cathode environment of polymer electrolyte membrane fuel cell, *Corrosion Science and Technology*, **21**, 340 (2022). Doi: https://doi.org/10.14773/cst.2022.21.5.340
11. D. H. Shin and S. J. Kim, Effects of thickness and defects of DLC coating layer on corrosion resistance of metallic bipolar plates of PEMFCs, *Corrosion Science and Technology*, **23**, 235 (2024). Doi: https://doi.org/10.14773/cst.2024.23.3.235
12. F. F. Chen, Y. Zhao, L. Liu, X. Li, and J. Zhang, Correlation between molecular features and electrochemical properties using an artificial neural network, *Materials and Design*, **112**, 410 (2016). Doi: https://doi.org/10.1016/j.matdes.2016.09.084
13. L. B. Coelho, D. Zhang, Y. Van Ingelgem, D. Steckelmacher, A. Nowé, and H. Terryn, Reviewing machine learning of corrosion prediction in a data-oriented perspective, *npj Materials Degradation*, **6**, 1 (2022). Doi: https://doi.org/10.1038/s41529-022-00218-4
14. X. Ding, C. Feng, P. Yu, K. Li, and X. Chen, Gradient boosting decision tree in the prediction of NOx emission of waste incineration, *Energy*, **264**, 126174 (2023). Doi: https://doi.org/10.1016/j.energy.2022.126174
15. X. Jiang, Y. Yan, and Y. Su, Data-driven pitting evolution prediction for corrosion-resistant alloys by time-series analysis, *npj Materials Degradation*, **6**, 2 (2022). Doi: https://doi.org/10.1038/s41529-022-00307-4
16. M. Längkvist, L. Karlsson, and A. Loutfi, A review of unsupervised feature learning and deep learning for time-series modeling, *Pattern Recognition Letters*, **42**, 11 (2014). Doi: https://doi.org/10.1016/j.patrec.2014.01.008

17. W. Wen, C. Wu, Y. Wang, Y. Chen, and H. Li, Learning structured sparsity in deep neural networks, *Advances in Neural Information Processing Systems* **29** (2016). https://papers.nips.cc/paper_files/paper/2016/hash/41bfd20a38bb1b0bec75acf0845530a7-Abstract.html
18. M. Aghaaminiha, H. Rastegar, S. Karami, and A. Bahrami, Machine learning modeling of time-dependent corrosion rates of carbon steel in presence of corrosion inhibitors, *Corrosion Science*, **193**, 109904 (2021). Doi: https://doi.org/10.1016/j.corsci.2021.109904
19. Y. Diao, L. Yan, and K. Gao, Improvement of the machine learning-based corrosion rate prediction model through the optimization of input features, *Materials and Design*, **198**, 109326 (2021). Doi: https://doi.org/10.1016/j.matdes.2020.109326
20. Y. Guang, W. Wang, H. Song, H. Mi, J. Tang, and Z. Zhao, Prediction of external corrosion rate for buried oil and gas pipelines: A novel deep learning method with DNN and attention mechanism, *International Journal of Pressure Vessels and Piping*, **209**, 105218 (2024). Doi: https://doi.org/10.1016/j.ijpvp.2024.105218
21. T. D. K. Thara, P. S. Prema, and F. Xiong, Auto-detection of epileptic seizure events using deep neural network with different feature scaling techniques, *Pattern Recognition Letters*, **128**, 544 (2019). Doi: https://doi.org10.1016/j.patrec.2019.10.029
22. Z. Li, Extracting spatial effects from machine learning model using local interpretation method: An example of SHAP and XGBoost, *Computers, Environment and Urban Systems*, **96**, 101845 (2022). Doi: https://doi.org/10.1016/j.compenvurbsys.2022.101845
23. J. Wu, X. Y. Chen, H. Zhang, L. D. Xiong, H. Lei, and S. H. Deng, Hyperparameter optimization for machine learning models based on Bayesian optimization, *Journal of Electronic Science and Technology*, **17**, 26 (2019). Doi: https://doi.org/10.11989/JEST.1674-862X.80904120
24. J. Gu, L. Zhang, W. Li, H. Zhao, and Y. Liu, Selection of key ambient particulate variables for epidemiological studies - Applying cluster and heatmap analyses as tools for data reduction, *Science of the Total Environment*, **435–436**, 541 (2012). Doi: https://doi.org/10.1016/j.scitotenv.2012.07.040
25. K. Mansouri, K. Ibrik, N. Bensalah, and A. Abdel-Wahab, Anodic dissolution of pure aluminum during electrocoagulation process: Influence of supporting electrolyte, initial pH, and current density, *Industrial & Engineering Chemistry Research*, **50**, 13362 (2011). Doi: https://doi.org/10.1021/ie201206d
26. K. H. Jung and S. J. Kim, Application of multiple linear regression to predict mechanical properties of 316L stainless steel with unspecified pit corrosion, *Corrosion Science and Technology*, **22**, 55 (2023). Doi: https://doi.org/10.14773/cst.2023.22.1.55
27. A. Kahyarian, A. Schumaker, B. Brown, and S. Nesic, Acidic corrosion of mild steel in the presence of acetic acid: Mechanism and prediction, *Electrochimica Acta*, **258**, 639 (2017). Doi: https://doi.org/10.1016/j.electacta.2017.11.109
28. B. Seo, H. K. Park, K. B. Park, H. S. Kang, and K. Park, Effect of hydrogen peroxide on Cr oxide formation of additive manufactured CoCr alloys during plasma electrolytic polishing, *Materials Letters*, **294**, 129736 (2021). Doi: https://doi.org/10.1016/j.matlet.2021.129736
29. M. Chang, J. Wu, D. Chen, and S. Ye, The composition of the rare earth based conversion coating formed on AZ91D magnesium alloy, *Corrosion Science and Technology*, **17**, 1 (2018). Doi: https://doi.org/10.14773/cst.2018.17.1.1
30. H. J. Flitt and D. P. Schweinsberg, Evaluation of corrosion rate from polarisation curves not exhibiting a Tafel region, *Corrosion Science*, **47**, 3034 (2005). Doi: https://doi.org/10.1016/j.corsci.2005.06.014
31. G. Mabilleau, S. Bourdon, M. L. Joly-Guillou, R. Filmon, M. F. Baslé, and D. Chappard, Influence of fluoride, hydrogen peroxide and lactic acid on the corrosion resistance of commercially pure titanium, *Acta Biomaterialia*, **2**, 121 (2006). Doi: https://doi.org/10.1016/j.actbio.2005.09.004
32. S. Salcedo-Sanz, J. L. Rojo-Álvarez, M. Martínez-Ramón, and G. Camps-Valls, Support vector machines in engineering: An overview, *Wiley Interdisciplinary Reviews: Data Mining and Knowledge Discovery*, **4**, 234 (2014). Doi: https://doi.org/10.1002/widm.1125
33. M. Aitkin and R. Foxall, Statistical modelling of artificial neural networks using the multi-layer perceptron, *Statistics and Computing*, **13**, 227 (2003). Doi: https://doi.org/10.1023/A:1024218716736
34. C. B. Aditya Satrio, W. Darmawan, B. U. Nadia, and N. Hanafiah, Time series analysis and forecasting of coronavirus disease in Indonesia using ARIMA model and PROPHET, *Procedia Computer Science*, **179**, 524 (2021). Doi: https://doi.org/10.1016/j.procs.2021.01.036
35. Y. S. Park and S. Lek, Artificial neural networks: Multilayer perceptron for ecological modeling, *Developments*

in Environmental Modelling, **28**, 123 (2016). Doi: https://doi.org/10.1016/B978-0-444-63623-2.00007-4

36. J. Rynkiewicz, General bound of overfitting for MLP regression models, *Neurocomputing*, **90**, 106 (2012). Doi: https://doi.org/10.1016/j.neucom.2011.11.028
37. Y. H. Fang, G. F. Wei, and Z. P. Liu, Catalytic role of minority species and minority sites for electrochemical hydrogen evolution on metals: Surface charging, coverage, and tafel kinetics, *Journal of Physical Chemistry C*, **117**, 7669 (2013). Doi: https://doi.org/10.1021/jp400608p
38. V. Vignal, H. Krawiec, O. Heintz, and R. Oltra, The use of local electrochemical probes and surface analysis methods to study the electrochemical behaviour and pitting corrosion of stainless steels, *Electrochimica Acta*, **52**, 4994 (2007). Doi: https://doi.org/10.1016/j.electacta.2007.01.079
39. V. Asghari, Y. F. Leung, and S. C. Hsu, Deep neural network based framework for complex correlations in engineering metrics, *Advanced Engineering Informatics*, **44**, 101058 (2020). Doi: https://doi.org/10.1016/j.aei.2020.101058
40. S. K. Sahu and R. N. Yadav, Key facial points recognition using ResNet, *Materials Today: Proceedings*, **66**, 3651 (2022). Doi: https://doi.org/10.1016/j.matpr.2022.07.342
41. X. Chen, T. Chen, Y. Cheng, W. Chen, A. Awadallah, and Z. Wang, Scalable learning to optimize: A learned optimizer can train big models, *European Conference on Computer Vision*, **13683**, 389 (2022). Doi: https://doi.org/10.1007/978-3-031-20050-2_23
42. Q. Tong, G. Liang, and J. Bi, Calibrating the adaptive learning rate to improve convergence of ADAM, *Neurocomputing*, **481**, 333 (2022). Doi: https://doi.org/10.1016/j.neucom.2022.01.014
43. R. Elshamy, O. Abu-Elnasr, M. Elhoseny, and S. Elmougy, Improving the efficiency of RMSProp optimizer by utilizing Nestrove in deep learning, *Scientific Reports*, **13**, 1 (2023). Doi: https://doi.org/10.1038/s41598-023-35663-x
44. X. Xie, P. Zhou, H. Li, Z. Lin, and S. Yan, Adan: Adaptive Nesterov momentum algorithm for faster optimizing deep models, *IEEE Transactions on Pattern Analysis and Machine Intelligence*, **46**, 9508 (2024). Doi: https://doi.org/10.1109/TPAMI.2024.3423382
45. Q. H. Nguyen, L. T. Tran, P. V. Pham, and T. T. Nguyen, Influence of data splitting on performance of machine learning models in prediction of shear strength of soil, *Mathematical Problems in Engineering*, **2021**, 4832864 (2021). Doi: https://doi.org/10.1155/2021/4832864
46. J. Liang, L. Hu, and J. Hao, Improvement of corrosion properties of microarc oxidation coating on magnesium alloy by optimizing current density parameters, *Applied Surface Science*, **253**, 6939 (2007). Doi: https://doi.org/10.1016/j.apsusc.2007.02.010
47. J. S. Lee, O. Baasanjav, J. S. Oh, and J. H. Lee, Time-dependent corrosion behavior of high chromium white cast iron in an acidic solution, *Corrosion Science and Technology*, **23**, 310 (2024). Doi: https://doi.org/10.14773/cst.2024.23.4.310
48. T. Domhan, J. T. Springenberg, and F. Hutter, *Proc. 24th IJCAI'15 Conf.*, pp. 3460 - 3468, *International Joint Conference on Artificial Intelligence (IJCAI)*, AAAI Press (2015). https://www.ijcai.org/Proceedings/15/Papers/487.pdf